



Synthesis of A2 and B2 Phases in $Al_xCoCrFeNi$ Multi-component System

M. Aizenshtein^{1,2} · S. Hayun¹

Received: 10 October 2019 / Revised: 16 April 2020 / Accepted: 22 April 2020 / Published online: 4 May 2020
© ASM International 2020

Abstract

The two phases of the $Al_xCoCrFeNi$ multi-component system, A2 ($Im\bar{3}m$, bcc) and B2 ($Pm\bar{3}m$, primitive) do not appear as single phases in the entire range studied to date ($0 < x < 3$). To measure the thermochemical properties of alloys and improve the accuracy of thermodynamic models, single phases need to be synthesized and characterized. Toward this end, we first study the mixture of A2 and B2 phases in the $Al_{2.75}CoCrFeNi$ multi-component alloy. After determining the composition of each phase, we attempted to synthesis each individual phase. The “B2” alloy is rich in Al, Ni, and Co and consists of a single primitive structure with a nonuniform composition. The “A2” alloy is a Cr- and Fe-rich alloy of compositional uniformity on the microscale, but that phase separates on the nanoscale into Al–Ni–Co-rich, nanometer-sized B2 precipitates in an A2 matrix rich in Cr and Fe. This result reveals the profound impact of Al on the stabilization of the B2 phase in the $Al_xCoCrFeNi$ system. Although the B2 alloy is adequate for thermochemical study, further efforts are required to synthesize an A2 alloy. In this case, the Al content should be less than 10 at.% and the Ni content should be about 1 at.%. These low contents of Al and Ni should prevent the formation of stable “Al–Ni-like” B2 ordered intermetallics.

Keywords $Al_xCoCrFeNi$ · Multi-component system · B2 ordered bcc · A2 disordered bcc

Introduction

High-entropy alloys, also known as multicomponent alloys or multi-principal-element alloys, consist of five or more elements of compositional fraction between 5 and 35 at.% [1]. These systems usually present two or more phases of simple crystallographic structure [e.g., face-centered cubic (fcc), body-centered cubic (bcc), or hexagonal close-packed (hcp)]. The high-entropy alloy system $Al_xCoCrFeNi$ has received significant research attention because of its superior mechanical properties and corrosion resistance vis-à-vis stainless steel [2–5]. Given its thermomechanical stability at elevated temperatures, it could be used to make improved thermal-barrier coatings [6].

In general, the $Al_xCoCrFeNi$ series is composed of a mixture of simple structures, such as fcc and bcc (the bcc

phase has an important role in hardening the alloy) [7]. The volume fraction of the bcc phase increases with increasing Al content and in many cases is a mixture of a disordered Fe- and Cr-rich bcc phase (A2) and an ordered Al- and Ni-rich bcc (B2) [8], both of which have a lattice parameter of 0.287 nm [9]. Although this system offers only simple crystal structures, the literature contains large discrepancies in the calculated phase diagram [10, 11] because of the limited availability of high-temperature experimental data. To determine the thermodynamic properties of the system, single phases must be synthesized and characterized by drop-solution calorimetry, differential thermal analysis, dilatometry, etc. (see, e.g., Refs. [12–14]). For this work, we synthesized single A2 and B2 phases that we initiated by determining the composition of each phase in a binary mixture of the phases in the alloy $Al_{2.75}CoCrFeNi$. After synthesis, the alloy microstructure, crystallographic structure, and composition were characterized by using X-ray diffraction (XRD), high-resolution scanning electron microscopy (HR-SEM), and transmission electron microscopy (TEM).

✉ M. Aizenshtein
aizensht@post.bgu.ac.il

¹ Department of Materials Engineering, Ben Gurion University of the Negev, Beersheba, Israel

² NRCN-Negev, Beersheba, Israel

Experimental Procedures

To determine the compositions of the A2 and B2 phases, an $\text{Al}_{2.75}\text{CoCrFeNi}$ alloy was prepared by using non-consumable electrode arc melting with a Ti-getter in an ultrahigh-purity argon atmosphere, as the first stage of the study. The raw materials (purity > 99.9%) were melted and turned over five times for improved homogeneity, followed by a last stage of arc-melting to a 6-mm-diameter rod. To coarsen the microstructure and reach compositional equilibrium, samples were cut from the cast rod, wrapped in tantalum foil, and sealed in quartz capsules. The samples were then heat-treated and quenched in water (Table 1). According to Ref. [11], for $x > 1.5$ and in the temperature range of 800–1300 °C, the $\text{Al}_x\text{CoCrFeNi}$ alloy contains a mixture of A2 and B2 phases, which assist us in determining the heat-treatment temperature.

The structure and composition of the phases thus obtained were characterized by using XRD, HR-SEM, and TEM. XRD analysis was done by using an Empyrean Alpha 1 diffractometer (Malvern Panalytical Ltd, Royston, UK) operated at 40 kV, 30 mA with Cu-K α radiation and $2\theta = 20^\circ$ to 120° with a step size of 0.02° and a scan step time of 1 s. The XRD patterns were analyzed by using a whole-pattern fitting approach with MDI Jade 2010 software (MDI, Livermore, CA, USA). Samples for SEM characterization were prepared by using SiC paper from 320 to 4000 grit and a final stage of polishing with 1 μm diamond paste. SEM images were acquired by using a Verios XHR 460L instrument equipped with a Noran Energy Dispersive spectrometer operated at 15 kV beam voltage. The TEM instrument (JEOL JEM-2100F, Peabody, MA, USA, operated at 200 kV) provided nanoscale structural information by selected area electron diffraction. The TEM sample was extracted from the surface of the SEM sample by using

Table 1 Heat treatments of $\text{Al}_{2.75}\text{CoCrFeNi}$ alloy

| Sample # | Heat treatment |
|----------|---|
| 1 | 1200 °C, 50 h, 1000 °C 25 h, quenched |
| 2 | 1200 °C, 50 h, 1000 °C 100 h, quenched |

Table 2 Composition of heat-treated samples determined by EDS

| Heat treatment (last isothermal temperature) | Al, at. % | Co, at. % | Cr, at. % | Fe, at. % | Ni, at. % |
|--|----------------|----------------|----------------|----------------|----------------|
| #1 | 39.4 ± 0.8 | 15.5 ± 0.9 | 14.2 ± 1.3 | 15.3 ± 0.4 | 15.5 ± 0.4 |
| #2 | 39.3 ± 1.3 | 14.9 ± 0.5 | 15.4 ± 0.9 | 15.4 ± 0.6 | 15.0 ± 0.2 |

a focused ion beam (FIB, Helios G4 UC, Thermo-Fisher Scientific, MA, USA).

In the second stage, as a function of the chemical composition determined by SEM energy dispersive spectrometry (EDS) combined with supplementary data from the literature, new alloys were prepared by arc-melting and then characterized in the same way as the synthesized alloys.

Results and Discussion

Characterization of Heat-Treated $\text{Al}_{2.75}\text{CoCrFeNi}$ Alloys

Table 2 presents the measured compositions of the heat-treated alloys, and Fig. 1 shows their microstructure. In both cases, the A2 phase (bright phase) precipitates from the B2 matrix in two ways: inside B2 grains with an equiaxial morphology and at grain boundaries with a high aspect ratio. Longer heat treatment results in coarsening the A2 phase at grain boundaries. Table 3 presents the composition of the A2 and B2 phases in the heat-treated samples.

In previous work, we found that the composition of the B2 phase depended on temperature between 900 and 1200 °C [15]. Table 4 summarizes the data and other published data on the composition of the A2 and B2 phases in the $\text{Al}_x\text{CoCrFeNi}$ system. The composition of the newly synthesized alloys was chosen based on the data given in Table 4.

Synthesis and Characterization of Al- and Ni-Rich and Cr- and Fe-Rich Alloys

Table 5 summarizes the compositions of the various alloys synthesized. The Cr- and Fe-rich alloy was prepared twice because the B2 phase appeared in the first alloy (see below). According to the definition of high-entropy alloys (i.e., the content of each element should exceed 5 at.%), we chose not to synthesize alloys with < 5% content of elements. As described in the introduction, if the A2 and B2 phases have the same lattice parameter, the most significant difference between XRD patterns of the two phases is an extra reflection (100) from the B2 phase (see Fig. 2).

Figure 3 presents the measured XRD patterns of the synthesized alloys, which show that the Cr–Fe rich1 alloy contains the B2 (100) reflection, whereas the Cr–Fe rich2 alloy contains less of this phase. Based on whole-pattern fitting, the content of the B2 phase in the Cr–Fe rich1 and Cr–Fe rich2 alloys is

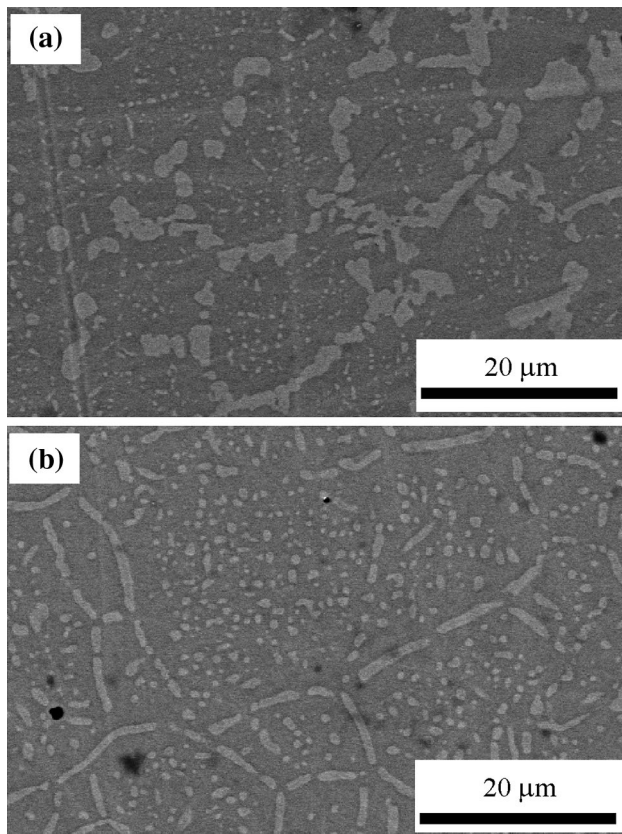


Fig. 1 BSE images of the heat-treated Al_{2.75}CoCrFeNi sample: (a) 1200 °C for 50 h, 1000 °C for 25 h, quenched; (b) 1200 °C for 50 h, 1000 °C for 100 h, quenched (A2 is bright phase, B2 is dark phase)

31 ± 2 and 24 ± 3 vol.%, respectively. The changes in composition and accompanying changes in lattice parameter shift the reflections (Table 6).

Since XRD is an integral measurement, the samples were imaged by SEM and TEM. A backscattered scattered electrons (BSE) image of the Al- and Ni-rich alloy shows clear compositional variance on the microscale (Fig. 4). The BSE image implies that compositional differences exist between the inner grains (dendrites) and the boundaries. Tables 7 and 8 summarize the SEM–EDS and TEM-EDS analyses. These results are consistent with the published results given in Table 4 (except for the Ni content in the bright phase). The results imply a transformation similar to the spinodal decomposition transformation of the B2 phase.

TEM electron diffraction confirms that the Al- and Ni-rich alloy contains a single primitive B2 structure. Figure 5 shows a forbidden $\bar{b}cc$ reflection and an allowed primitive reflection from (111) when the zone axis is along [112]. This pattern exists in the core and at grain boundaries. The lattice parameter *a* extracted from the electron patterns and from the patterns with the [111] zone axis is 0.2918 ± 0.0006 nm in the core and 0.2912 ± 0.0005 nm at the boundaries. Electron diffraction detects only minor differences between the two regions, and these results for the lattice parameter are slightly greater than those extracted from the XRD pattern (Table 6). Thus, despite the significant compositional differences between the two regions, the lattice parameters are practically identical (within instrumental error).

The low-magnification BSE images of the Cr–Fe rich2 sample (Fig. 6) show the grain structure and the relatively

Table 3 Composition of A2 and B2 phases (as determined by SEM–EDS measurements) of heat-treated samples

| Heat treatment | Al, at.% | Co, at.% | Cr, at.% | Fe, at.% | Ni, at.% |
|--------------------------------|------------|------------|------------|------------|------------|
| <i>A2 phase</i> | | | | | |
| 1200 °C_50 h, 1000 °C_ 100 h_q | 21.6 ± 0.3 | 5.3 ± 0.2 | 47.8 ± 0.5 | 23.0 ± 0.4 | 2.4 ± 0.2 |
| <i>B2 phase</i> | | | | | |
| 1200 °C_50 h, 1000 °C_ 25 h_q | 44.2 ± 0.1 | 17.9 ± 0.4 | 5.8 ± 0.2 | 12.8 ± 0.4 | 19.3 ± 0.1 |
| 1200 °C_50 h, 1000 °C_ 100 h_q | 44.2 ± 0.2 | 17.5 ± 0.4 | 6.6 ± 0.5 | 13.0 ± 0.1 | 18.7 ± 0.4 |

Volume of interaction is too large for measurement of single A2 phase in the 1200 °C_50 h, 1000 °C_ 25 h_q sample

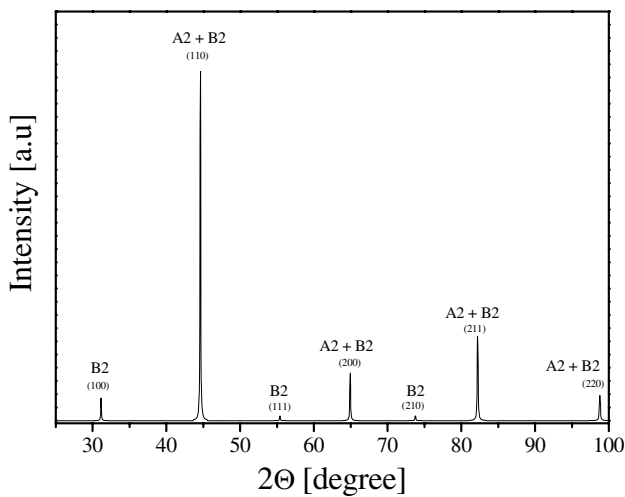
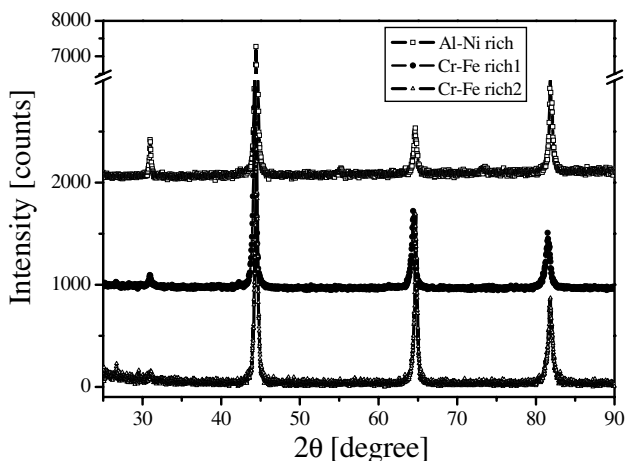
Table 4 Published compositions of A2 and B2 phases

| Referennces | Al, at.% | Co, at.% | Cr, at.% | Fe, at.% | Ni, at.% |
|----------------------------|------------|------------|------------|------------|-----------|
| <i>A2 Phase</i> | | | | | |
| [5] (for <i>x</i> = 1) | 3 | 19 | 43 | 30 | 6 |
| [11] (for <i>x</i> = 1.5) | 5.0 ± 1.0 | 8.8 ± 0.6 | 52.9 ± 4.0 | 31.8 ± 4.8 | 1.1 ± 0.8 |
| [15] (for <i>x</i> = 2.75) | 16.6–30.9 | 5.3–8.5 | 34.2–47.8 | 19.8–27.5 | 2.4–6.6 |
| <i>B2 Phase</i> | | | | | |
| [5] (for <i>x</i> = 1) | 30 | 19 | 9 | 14 | 27 |
| [11] (for <i>x</i> = 1.5) | 40.2 ± 2.6 | 21.3 ± 2.1 | 3.2 ± 1.1 | 11.2 ± 0.8 | 24 ± 5.3 |
| [15] (for <i>x</i> = 2.75) | 42.2–46.8 | 17.3–17.6 | 5.5–8.8 | 12.4–14 | 17.8–18.6 |

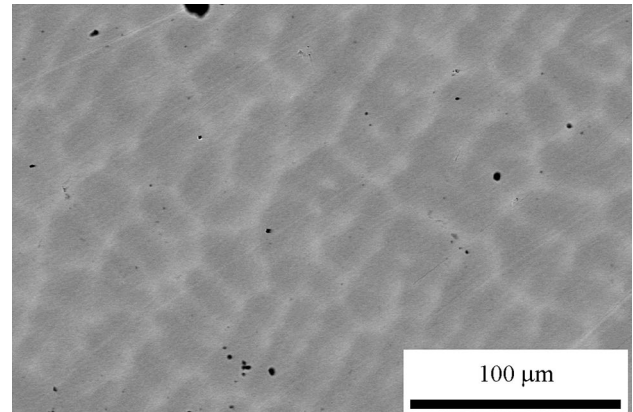
Table 5 Composition of synthesized alloys (area EDS measurements)

| Alloy | Al, at. % | Co, at. % | Cr, at. % | Fe, at. % | Ni, at. % |
|---------------------|------------|------------|------------|------------|-----------|
| Al–Ni rich (n) | 38 | 20 | 6 | 12 | 24 |
| Al–Ni rich (m) | 38.0 ± 0.1 | 20.3 ± 0.2 | 5.9 ± 0.1 | 11.8 ± 0.1 | 24 ± 0.3 |
| Cr–Fe rich 1 (n) | 21 | 7 | 42 | 25 | 5 |
| Cr–Fe rich 1 (m) | 19.6 ± 0.3 | 7.5 ± 0.1 | 42.4 ± 0.6 | 25.6 ± 0.4 | 4.9 ± 0.4 |
| Cr–Fe rich 2 (n) | 15 | 8 | 45 | 27 | 5 |
| Cr–Fe rich 2 (m) | 14.7 ± 0.2 | 8.6 ± 0.4 | 44.3 ± 0.3 | 27.3 ± 0.2 | 5.1 ± 0.3 |

n nominal, *m* measured

**Fig. 2** Theoretical XRD pattern of powder A2+50 vol.% B2 phases using Cu-K α radiation**Fig. 3** Experimental XRD patterns of synthesized alloys**Table 6** Lattice parameters of the three synthesized alloys extracted by the whole pattern fitting analysis of the XRD data

| Alloy | Structure (main phase) | Lattice parameter, nm |
|-------------|------------------------|-----------------------|
| Al–Ni rich | Ordered bcc | 0.2878 ± 0.0001 |
| Cr–Fe rich1 | Disordered bcc | 0.2888 ± 0.0003 |
| Cr–Fe rich2 | Disordered bcc | 0.2882 ± 0.0001 |

**Fig. 4** BSE image of Al–Ni-rich alloy, showing compositional differences between core and grain boundaries (i.e., dendrites)**Table 7** SEM–EDS analysis of Al- and Ni-rich alloy

| | Al, at. % | Co, at. % | Cr, at. % | Fe, at. % | Ni, at. % |
|--------------|------------|------------|------------|------------|------------|
| Bright phase | 32.0 ± 1.0 | 20.8 ± 0.2 | 10.3 ± 1.0 | 17.7 ± 1.0 | 19.2 ± 0.9 |
| Dark phase | 41.1 ± 0.9 | 19.7 ± 0.3 | 3.8 ± 0.5 | 9.5 ± 1.0 | 25.9 ± 0.5 |

Table 8 TEM–EDS analysis of Al- and Ni-rich alloy

| | Al, at. % | Co, at. % | Cr, at. % | Fe, at. % | Ni, at. % |
|--------------|------------|------------|-----------|------------|------------|
| Bright phase | 31.4 ± 0.2 | 21.3 ± 0.6 | 9.1 ± 0.6 | 16.3 ± 0.7 | 21.9 ± 0.4 |
| Dark phase | 42.1 ± 0.6 | 19.2 ± 0.6 | 4.1 ± 0.4 | 9.3 ± 0.2 | 25.3 ± 0.3 |

large grain size (≈ 200 – $300 \mu\text{m}$), with a finer periodic morphology detected inside the grains. Higher magnification reveals nanoprecipitates.

Figures 7 and 8 show TEM images of samples prepared by FIB. These images prove that the alloy is a mixture of A2 (matrix) and B2 (precipitate). Again, the X-ray mapping shows that the primitive B2 phase is richer in Al, Co, and Ni whereas the A2 bcc phase is richer in Cr and Fe. Table 9 summarizes the results of EDS elemental analysis of the $\approx 50 \text{ nm}$ B2 precipitate.

Based on these results and the nominal composition of the alloy, we calculated the volume fraction of each phase

Fig. 5 (a) Bright-field TEM image of Al-Ni-rich alloy. Electron diffraction shows that sample has a primitive structure both (b) in the core and near grains and (c) boundaries

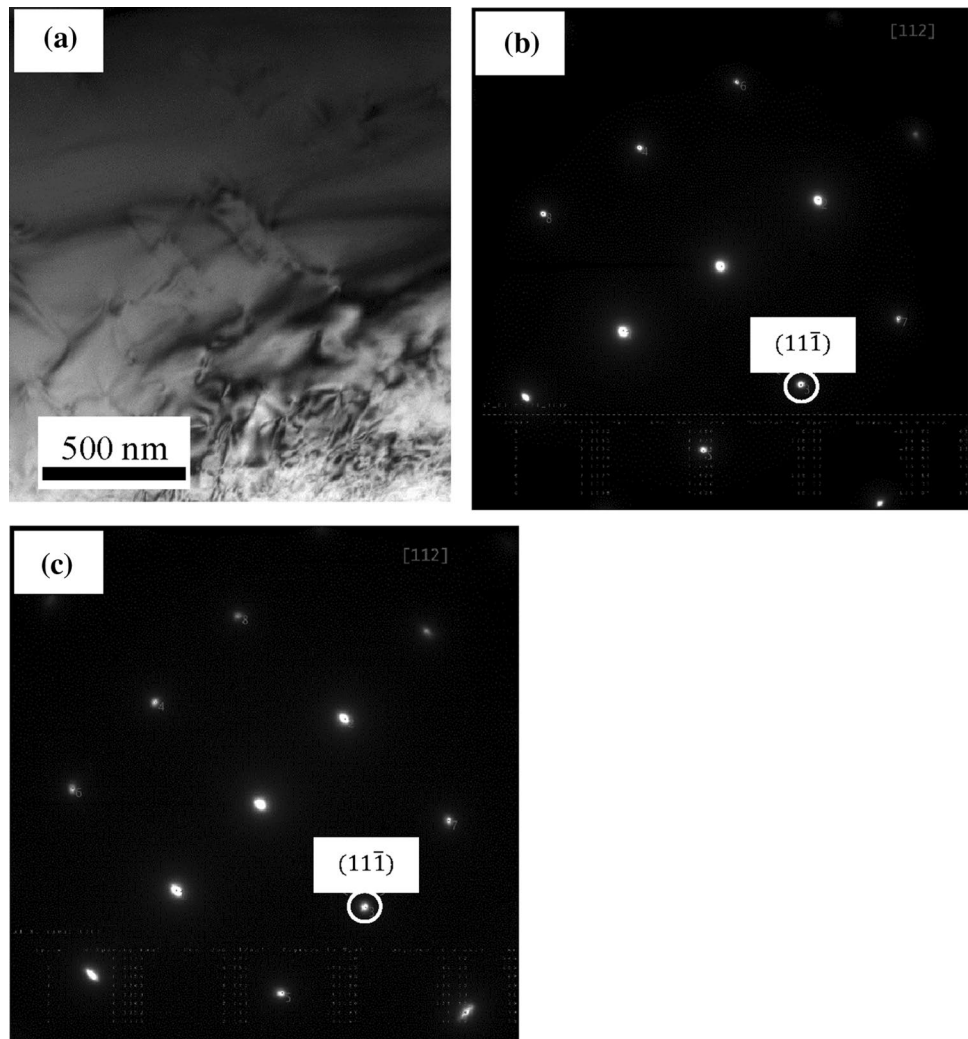
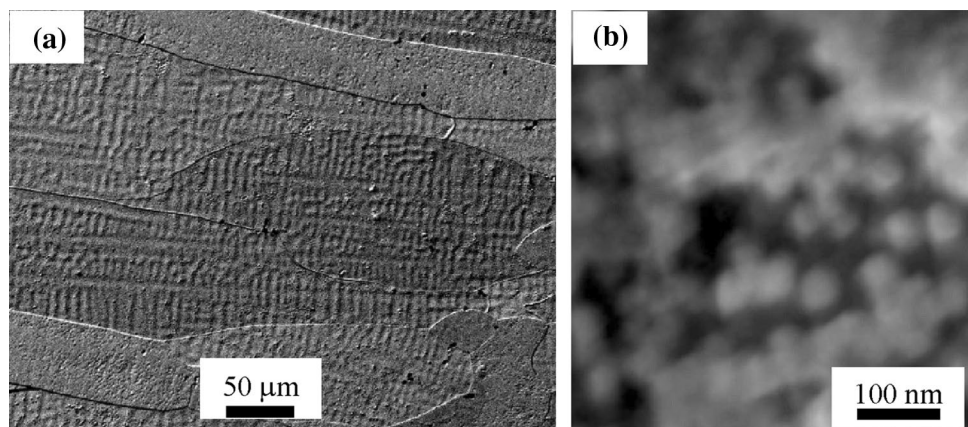


Fig. 6 BSE image of the Cr-Fe rich2 sample after 30 s etching by aqua regia solution at different magnifications (a) grain size is emphasized (b) nano-sized precipitate inside grains



in the sample and obtained 0.72 ± 0.05 and 0.28 ± 0.05 for the A2 and B2 phases, respectively. These results are reasonably consistent with the XRD analysis. Furthermore, the data reported in Table 9 could help to evaluate the

order parameter η of the B2 phase. The B2 phase contains two sub-lattices; 1a (for $\eta = 1$, the sub-lattice occupied by Co, Cr, Fe, and Ni) and 1b (for $\eta = 1$, the sub-lattice occupied by Al). Assuming that all Al atoms occupy the 1b sub-lattice leads to the equation [16]

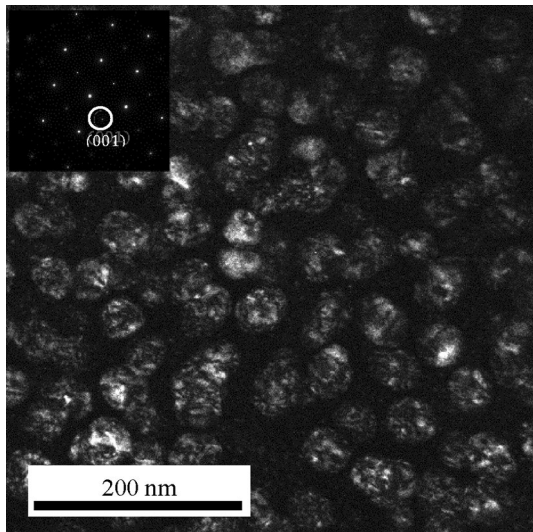


Fig. 7 Dark-field image from (001) reflection, which is allowed for primitive structure and forbidden for bcc structure. Image shows ≈ 50 nm B2 precipitate in A2 matrix

$$C_{1b} = 0.5(1 + \eta), \quad (1)$$

where C_{1b} is the occupancy of sub-lattice 1b by Al atoms. Given $C_{1b} = 0.333/0.5$, then $\eta = 0.33$.

The Cr, Fe, and Ni contents of the A2 phase are consistent with Ref. [17], which means that a single-phase A2 alloy would be stabilized if the Al content were reduced below 10 at.%. Therefore, to minimize the B2 content, an alloy should be synthesized with low Al and Ni content (≈ 1 at.%). Note that Al and Ni have high affinity to each other, as seen in the high-temperature stable AlNi (B2) ordered intermetallic [18].

Summary and Conclusions

The goal of this study was to synthesize single A2 and B2 phases, which exist as a mixture in the $Al_xCoCrFeNi$ multi-component system. To determine the desired compositions, an $Al_{2.75}CoCrFeNi$ alloy was held at high temperatures for long periods to coarsen the microstructure. The composition of each phase was determined by SEM–EDS analysis and synthesized together by using arc-melting. Characterization

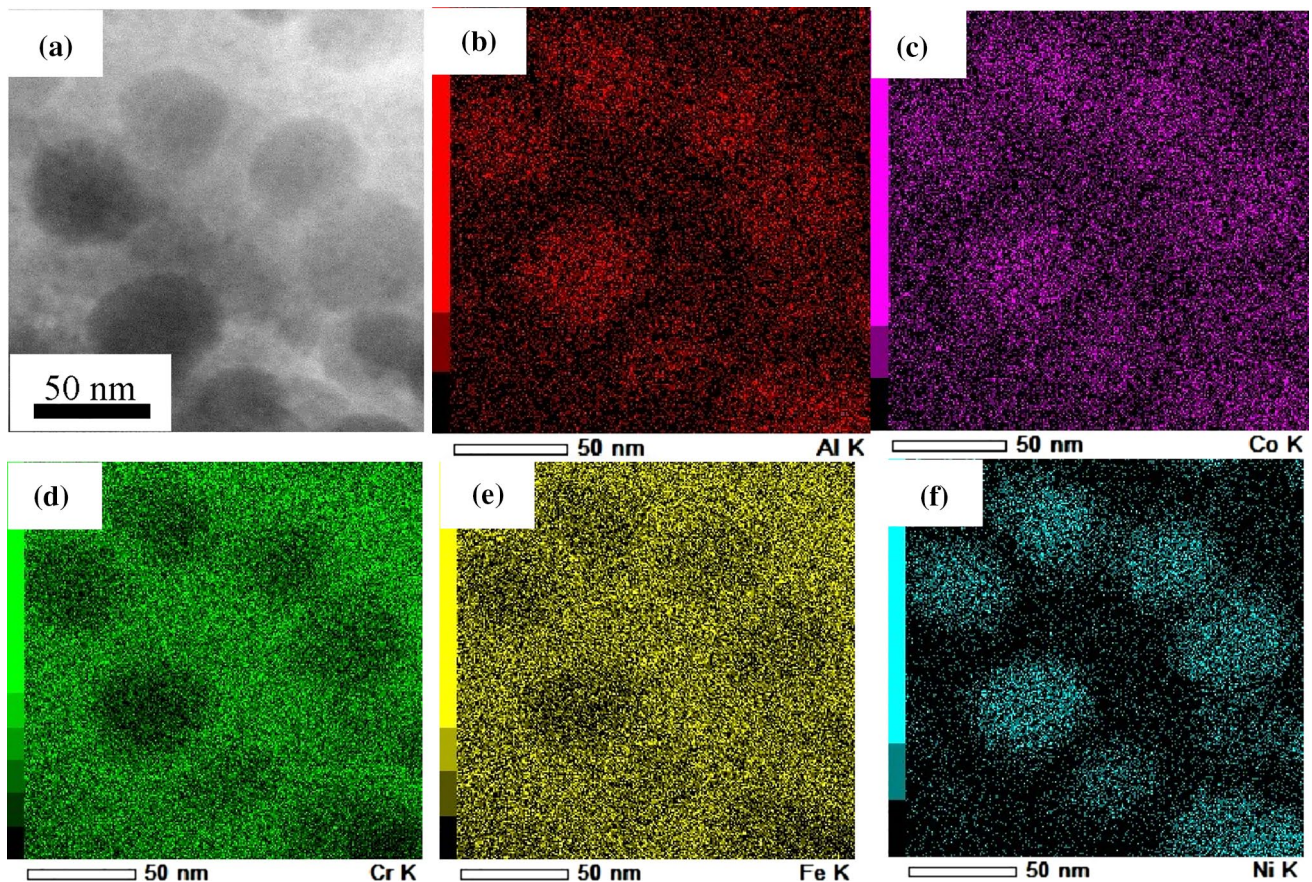


Fig. 8 (a) STEM image and (b)–(f) EDS X-ray mapping. The B2 phase is rich in Al, Co, and Ni compared with the A2 matrix

Table 9 TEM-EDS of A2 matrix and B2 precipitate

| Alloy | Al, at. % | Co, at. % | Cr, at. % | Fe, at. % | Ni, at. % |
|----------------|------------|-----------|------------|------------|------------|
| A2 matrix | 10.5 ± 0.6 | 5.4 ± 0.1 | 53.8 ± 0.8 | 29.2 ± 0.2 | 1.1 ± 0.4 |
| B2 precipitate | 33.3 ± 2.5 | 13.5 ± 1 | 21.4 ± 3 | 16.3 ± 1.5 | 15.5 ± 1.8 |

of the alloys reveals that the A2 alloy is homogeneous on the microscale but not on the nanoscale where nanometer-sized B2 precipitate forms. The results also reveal a single B2 alloy with compositional variance on the microscale. Despite compositional variations in the B2 alloy, it could be used for further thermochemical research, whereas the “A2” alloy should be refined to a single (A2) phase by reducing the Al content below 10 at.% and the Ni content to about 1 at.%. These low Al and Ni contents should prevent the formation of stable “Al-Ni-like” ordered intermetallics.

References

- J.W. Yeh, S.K. Chen, S.J. Lin, J.Y. Gan, T.S. Chin, T.T. Shun, C.H. Tsau, S.Y. Chang, Nanostructured high-entropy alloys with multiple principal elements: novel alloy design concepts and outcomes. *Adv. Eng. Mater.* **6**(5), 299–303 (2004)
- Y.Y. Chen, T. Duval, U.D. Hung, J.W. Yeh, H.C. Shih, Microstructure and electrochemical properties of high entropy alloys—a comparison with type-304 stainless steel. *Corros. Sci.* **47**(9), 2257–2279 (2005)
- C.W. Tsai, M.H. Tsai, J.W. Yeh, C.C. Yang, Effect of temperature on mechanical properties of Al_{0.5}CoCrCuFeNi wrought alloy. *J. Alloys. Compd.* **490**(1–2), 160–165 (2010)
- C.J. Tong, M.R. Chen, S.K. Chen, J.W. Yeh, T.T. Shun, S.J. Lin et al., Mechanical performance of the Al_xCoCrCuFeNi high-entropy alloy system with multiprincipal elements. *Metall. Mater. Trans. A.* **36**, 1263–1271 (2005)
- Y. Lu, Y. Dong, S. Guo, L. Jiang, H. Kang, T. Wang, B. Wen, W. Zhijun, J.C. Jie, Z. Cao, H.H. Ruan, L. Tingju, A promising new class of high-temperature alloys: eutectic high-entropy alloys. *Sci. Rep.* **4**, 6200 (2015). <https://doi.org/10.1038/srep06200>
- A.S.M. Ang, C.C. Berndt, M.L. Sesso, A. Anupam, P.S.R.S. Kottada, B.S. Murty, Plasma-sprayed high entropy alloys: microstructure and properties of AlCoCrFeNi and MnCoCrFeNi. *Metall. Mater. Trans. A* **46**, 791–800 (2015)
- W.R. Wang, W.L. Wang, S.C. Wang, Y.C. Tsai, C.H. Lai, J.W. Yeh, Effects of Al addition on the microstructure and mechanical property of Al_xCoCrFeNi high-entropy alloys. *Intermetallics* **26**, 44–51 (2012)
- Y.F. Kao, T.J. Chen, S.K. Chen, J.W. Yeh, Microstructure and mechanical property of as-cast, -homogenized, and -deformed Al_xCoCrFeNi (0 ≤ x ≤ 2) high entropy alloys. *J. Alloy. Compd.* **488**(1), 57–64 (2009)
- Z. Tang, O.N. Senkov, C.M. Parish, C. Zhang, F. Zhang, L.J. Santodonato, G. Wang, G. Zhao, F. Yang, P.K. Liawa, Tensile ductility of an AlCoCrFeNi multi-phase high-entropy alloy through hot isostatic pressing (HIP) and homogenization. *Mater. Sci. Eng. A* **647**, 229–240 (2015)
- C. Zhang, F. Zhang, S. Chen, W. Cao, Computational dynamics aided high-entropy alloy design. *JOM* **64**(7), 839–845 (2012)
- C. Zhang, M.C. Gao, CALPHAD modeling of high-entropy alloys, in *High-Entropy Alloys Fundamentals and Applications*, ed. by M.C. Gao, J.W. Yeh, P.K. Liaw, Y. Zhang (Springer, Switzerland, 2016), p. 422
- S.V. Kim, P. Meschel, W. Nash, Chen, Experimental formation enthalpies for intermetallic phases and other inorganic compounds. *Sci. Data* **4**, 170162 (2017)
- A. Belgacem-Bouzida, Y. Djaballah, M. Notin, Calorimetric measurement of the intermetallic compounds Cr₃Ga and CrGa₄ and thermodynamic assessment of the (Cr–Ga) systems. *J. Alloys Compd.* **397**(1–2), 155–160 (2005)
- S. Chatain, C. Gueneau, D. Labroche, O. Dugne, J. Rogez, Thermodynamic assessment of the Fe–U binary system. *JPE* **24**(2), 122–131 (2003)
- M. Aizenshtein, E. Strumza, E. Brosh, S. Hayun, Precipitation kinetics, microstructure and equilibrium state of the A2 and B2 phases in the multi component Al_{2.75}CoCrFeNi alloy. *J. Mater. Sci.* **55**, 7016–7028 (2020)
- A. Loiseau, C. Ricolleau, L. Potez, F. Ducastelle, Order and disorder at interfaces of Alloys, in *Advances in Physical Metallurgy*, ed. by S. Banerjee, R.V. Ramanujan (Gordon and Breach Publishers, The Netherlands, 1996), p. 170
- T. Yang, S. Xia, S. Liu, C. Wang, S. Liu, Y. Fang, Y. Zhang, J. Xue, S. Yan, Y. Wang, Precipitation behavior of Al_xCoCrFeNi high entropy alloys under ion irradiation. *Sci. Rep.* **6**, 32146 (2016)
- I. Ansara, N. Dupin, H.L. Lukas, B. Sundman, Thermodynamic assessment of the Al–Ni system. *J. Alloys Compd.* **247**(1–2), 20–30 (1997)

Publisher's Note Springer Nature remains neutral with regard to jurisdictional claims in published maps and institutional affiliations.